4.5.4 Pulsed Laser Method

Silver nitrate+ reducing agent -----> Silver nanoparticle

heating

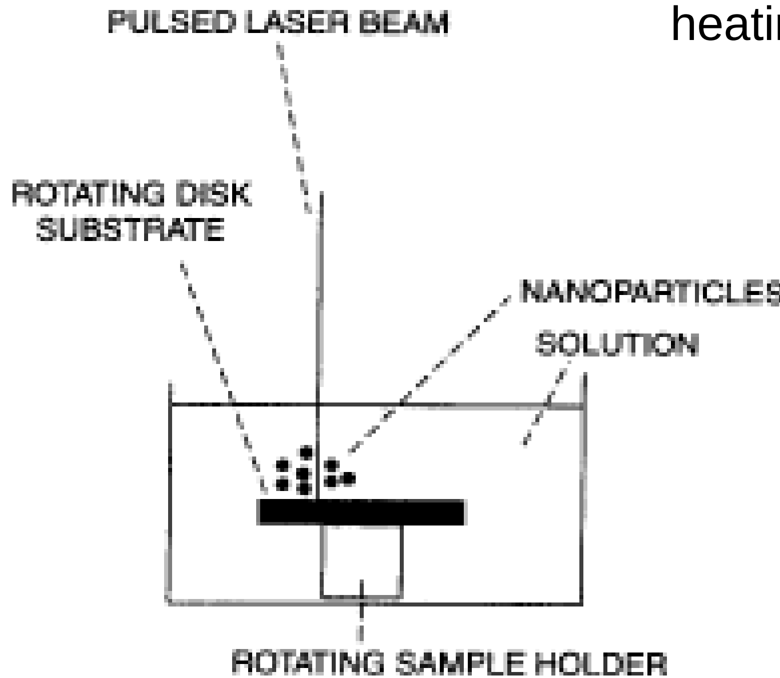

Figure 4.28. Apparatus to make silver nanoparticles using a pulsed laser beam that creates hot spots on the surface of a rotating disk. [Adapted from J. Singh, *Mater. Today* 2, 10 (2001).]

Laser Ablation

Laser Ablation

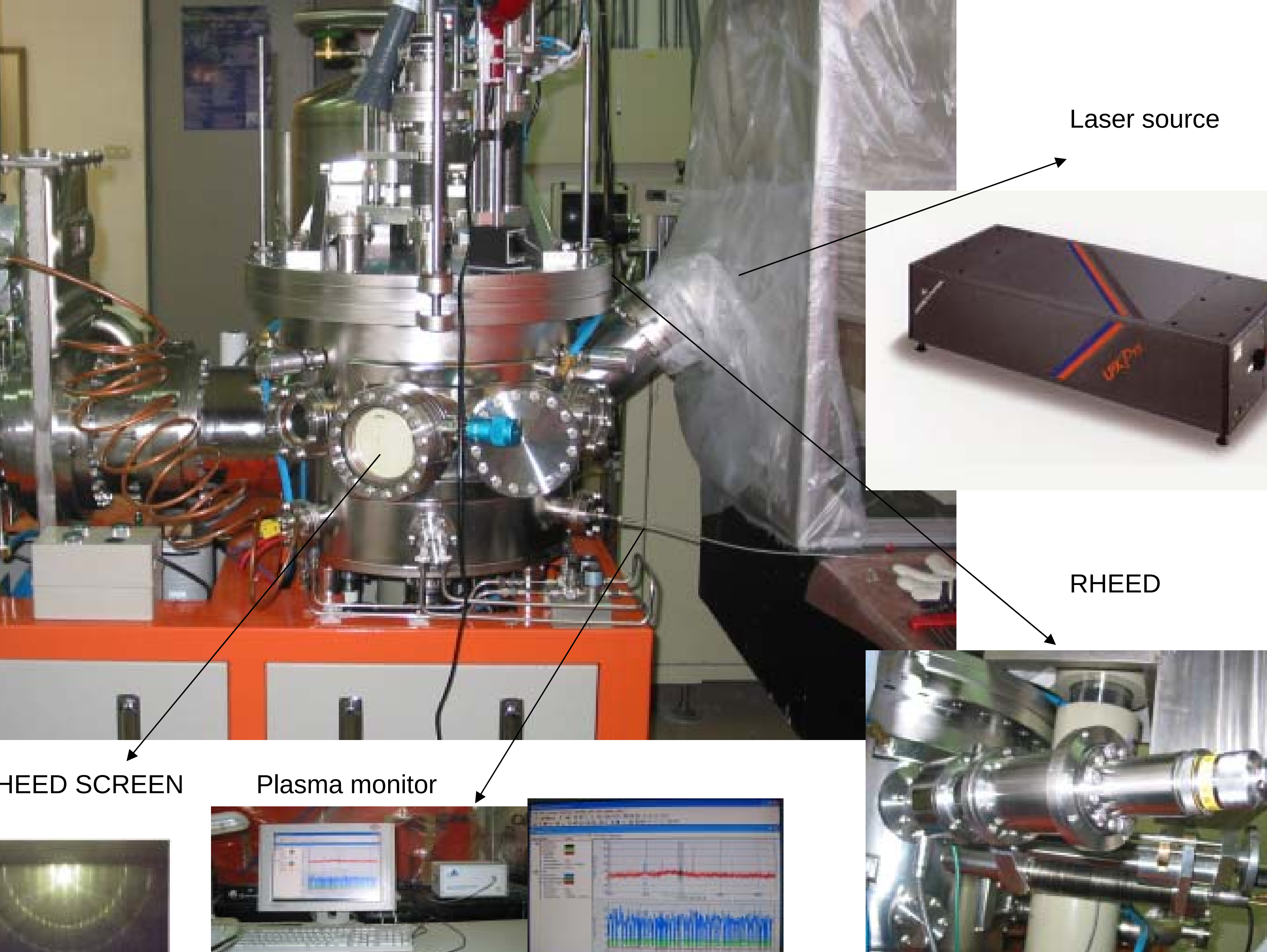
Laser source
RHEED
HEED SCREEN
Plasma monitor

1. Quantum size effects on the competition between Kondo interaction and magnetic order in 0-D.

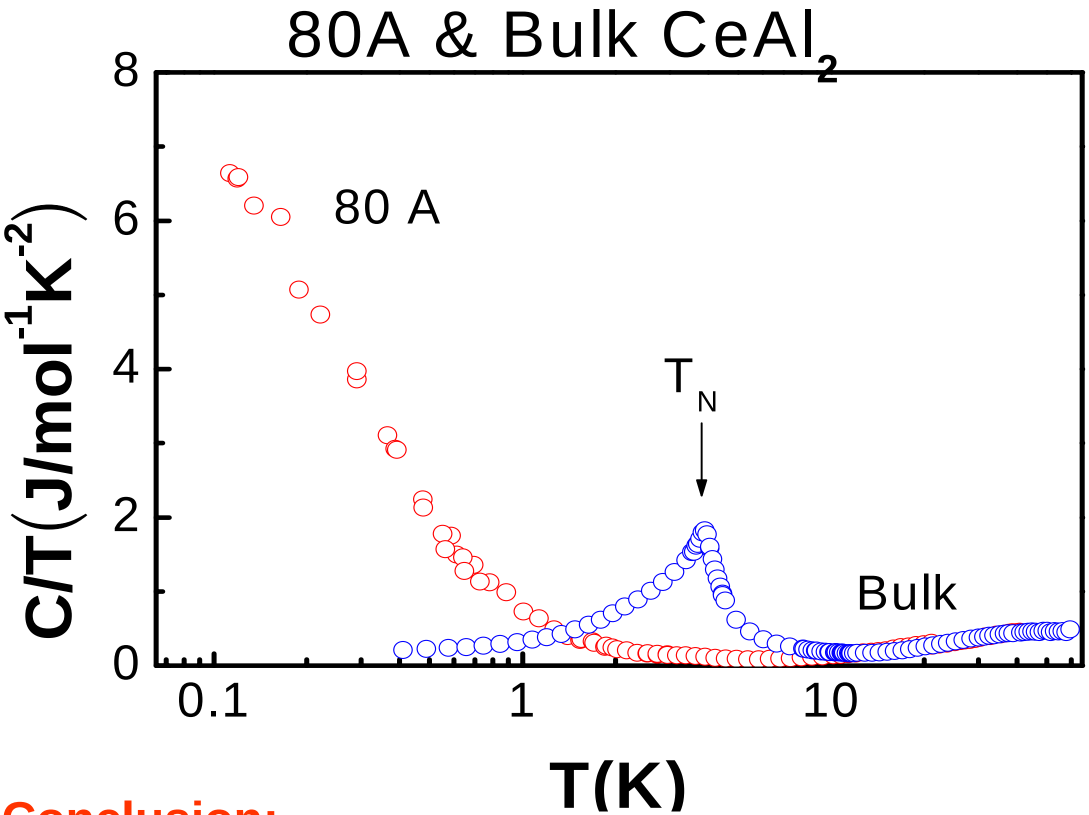

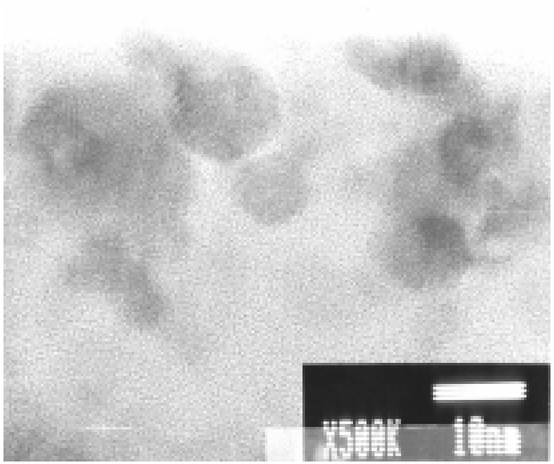

Conclusion:

In 80A -$CeAl_2$, magnetic ordering completely disappears and the γ reaches 9500 mJ/mol Ce K^2.

Unsolved problems:

In nanoparticle, only 0.7 Mole Ce^{3+} left, Is the 0.3 mol non-magnetic Ce really on the surface ? or it is just a coincidence.

4.6 Conclusion

In this chapter a number of examples have been presented showing that the physical, chemical, and electronic properties of nanoparticles depend strongly on the number and kind of atoms that make up the particle. We have seen that color, reactivity, stability, and magnetic behavior all depend on particle size. In some instances entirely new behavior not seen in the bulk has been observed such as magnetism in clusters that are constituted from nonmagnetic atoms. Besides providing new

Chapter 6 Bulk Nanostructured Materials

- Bulk nanostructured materials are solid
- having
- 1. a nanosized microstructure
- 2. the basic units are nanoparticles

Hypothetical 2-D
Oedered –Al_{12} particles
forming nanostructure

Disordered Al_{12} Particles

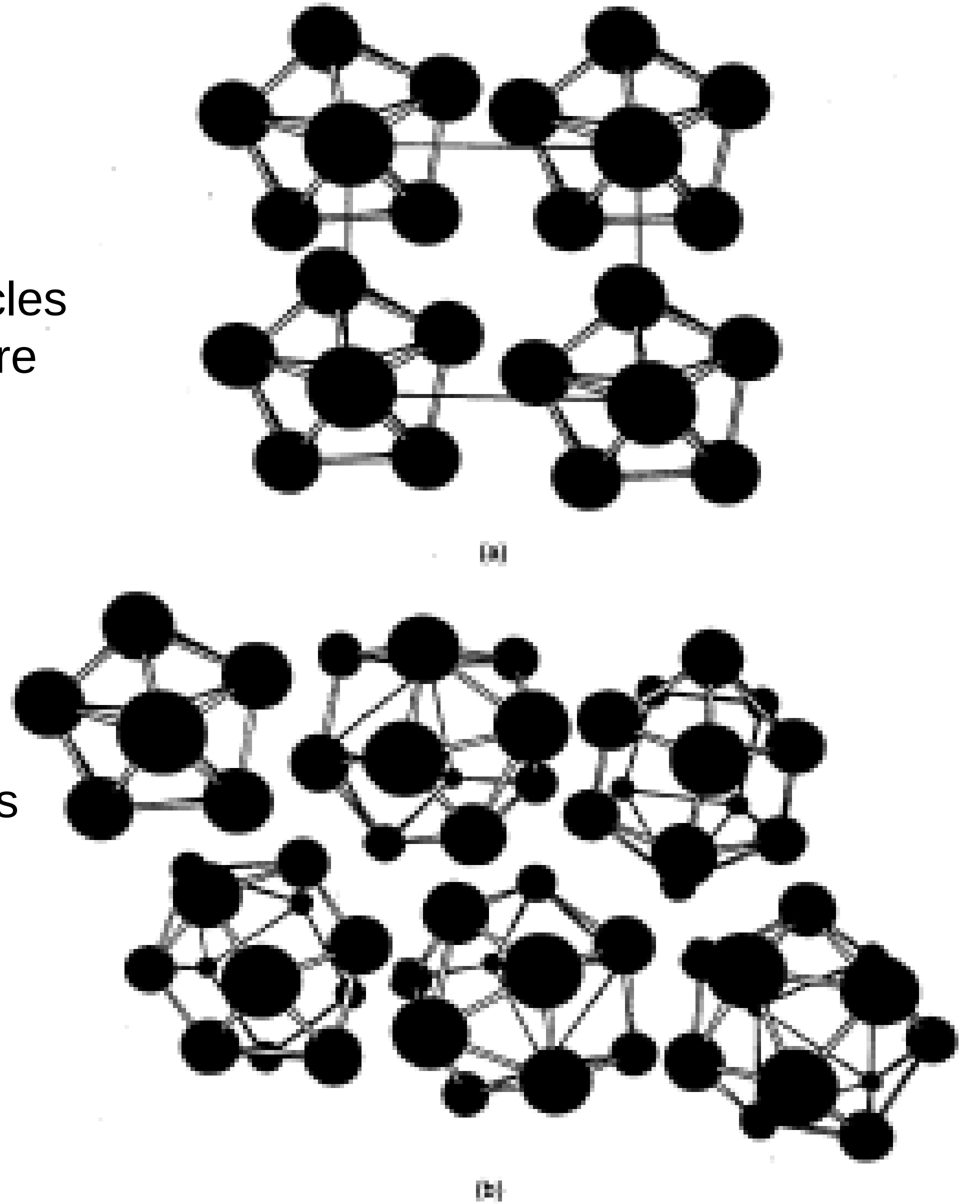

Figure 6.1. (a) Illustration of a hypothetical two-dimensional square lattice of Al_{12} particles, and (b) illustration of a two-dimensional bulk solid of Al_{12} where the nanoparticles have no ordered arrangement with respect to each other.

6.1 Solid disordersed nanostructure

- Compaction and consolidation
- 1. 85%Cu and 15%Fe powder in atomic weight
- 2. Ball milling to form $Fe_{85}Cu_{15}$ particles
- 3. Compacted using a tungsten-carbide at 1GPa
- 4. Hot compaction at ~ 400C with 870 MPa
- Density 99.2%

Distribution of size

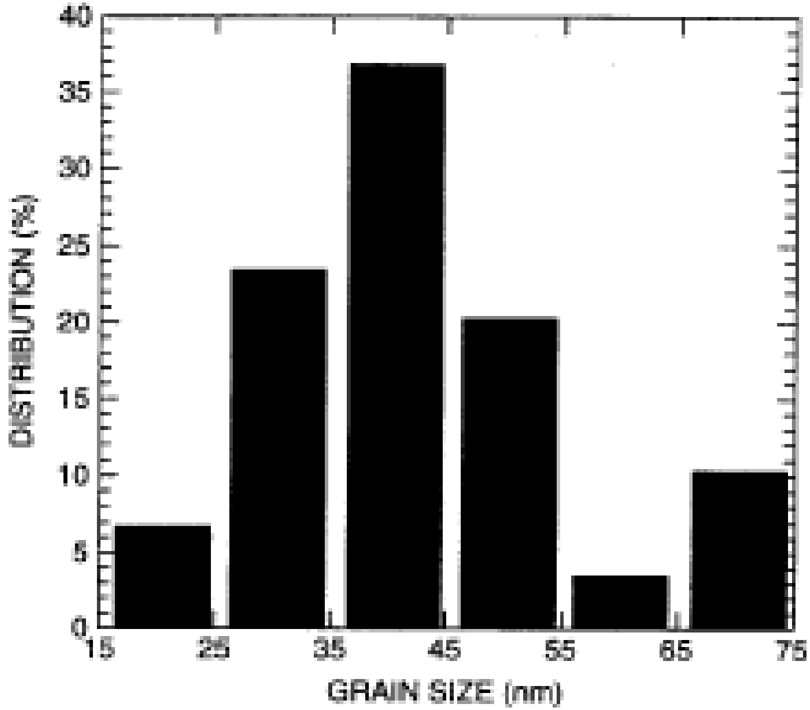

Figure 6.2. Distribution of sizes of Fe–Cu nanoparticles made by hot compaction methods described in the text. [Adapted from L. He and E. Ma, *J. Mater. Res.* **15**, 904 (2000).]

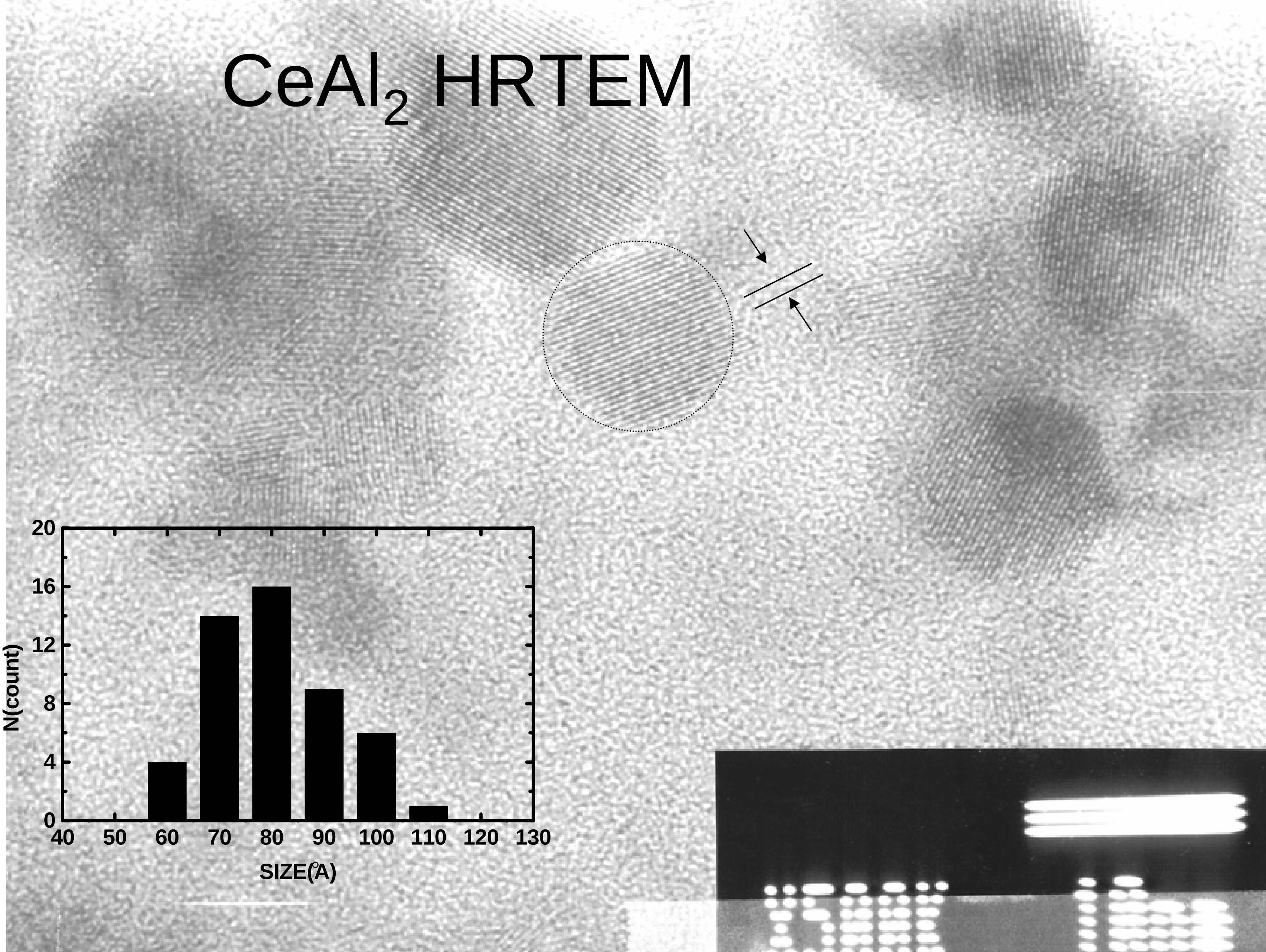
CeAl2 HRTEM
N(count)
0
4
8
12
16
20
40 50 60 70 80 90 100 110 120 130
SIZE(Å)

Fracture stress enhanced from 0.56 GPa (40 nm grain) to 2.8 GPa (50-150 um grain Iron)

Ductile region

Young's modulus

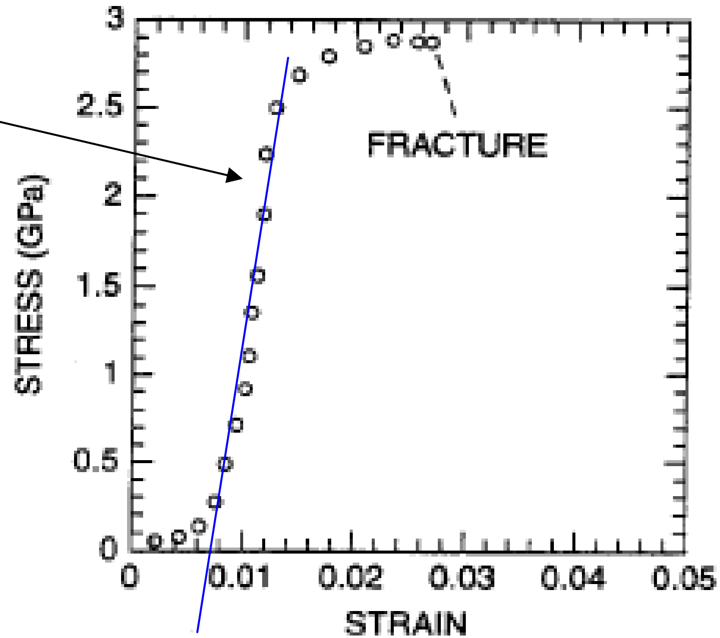

ure 6.3. Stress–strain curve for bulk compacted nanostructured Fe–Cu material, showing ture at a stress of 2.8 GPa. [Adapted from L. He and E. Ma, *J. Mater. Res.* **15**, 904 (2000).]

Ductile?柔軟
Brittle? 脆

Rapid solidfication-Chill block melt spinning

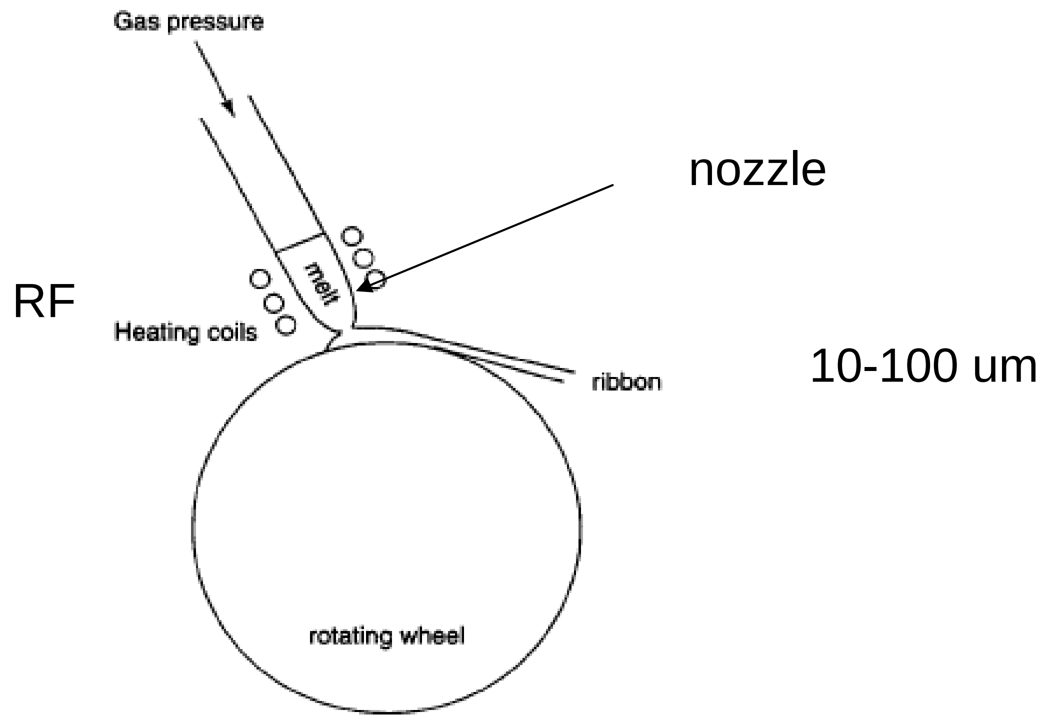

Figure 6.4. Illustration of the chill block melting apparatus for producing nanostructured materials by rapid solidification on a rotating wheel. (With permission from I. Chang, in *Handbook of Nanostructured Materials and Nanotechnology*, H. S. Nalwa, ed., Academic Press, San Diego, 2000, Vol. 1, Chapter 11, p. 501.)

Light weight, high strength materials

- 1. A melt spun alloy Al(85-94%)-Y-Ni-Fe
- 2. Consisting of 10-30 nm Al particles
- 3. Tensile strength ~1.2 GPa

Gas atomization

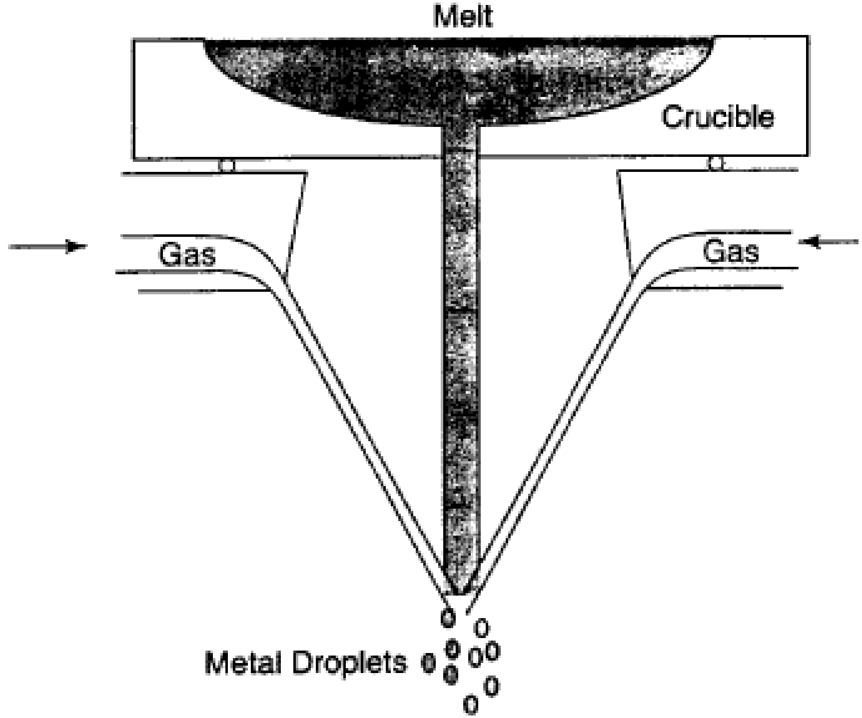

Figure 6.5. Illustration of apparatus for making droplets of metal nanoparticles by gas atomization. (With permission from I. Chang, in *Handbook of Nanostructured Materials and Nanotechnology*, H. S. Nalwa, ed., Academic Press, San Diego, 2000, Vol. 1, Chapter 11, p. 501.)

Electrodeposition (P137)

- Electrodes
- Electrolyte (電解液)
- Cu 2 mm film with grain size of 27 nm
- Enhanced yield strength 119 MPa

6.1.2 Failure mechanisms of conventional grain-sized materials

Crack!

An irreversible elongation after breaking of the bond

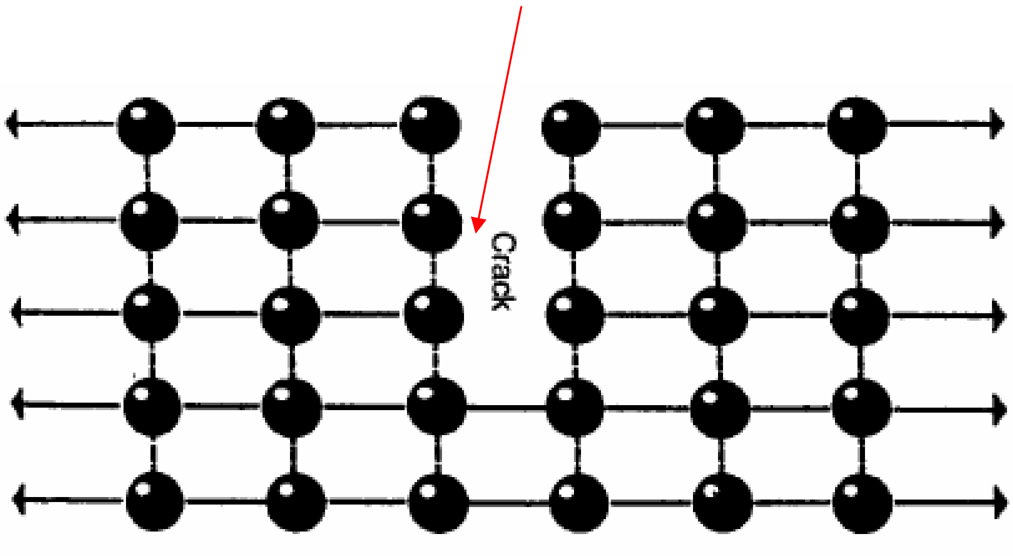

Figure 6.6. A crack in a two-dimensional rectangular lattice.

Brittle to ductile transition !

B to D region

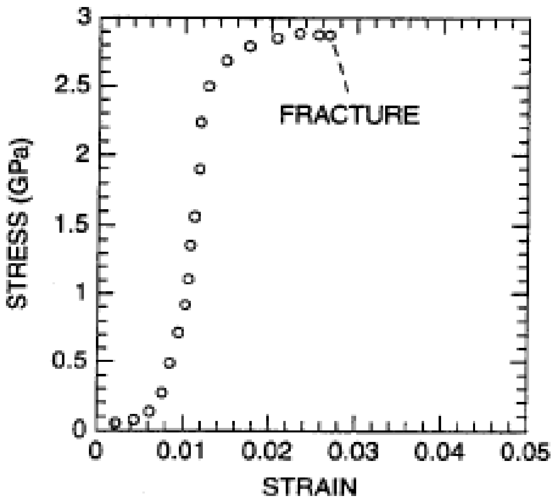

-strain curve for bulk compacted nanostructured Fe–
of 2.8 GPa. [Adapted from L. He and E. Ma, *J. Mater.*

Lattice dislocation.

1. Lattice slide
2. Weaker bonds along the dislocation

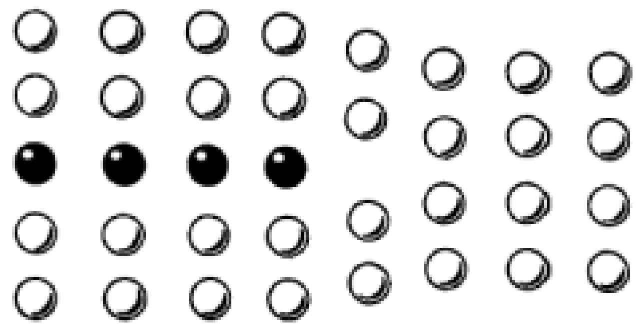

Figure 6.7. An edge dislocation in a two-dimensional rectangular lattice.

Hardening: to Impede the movement of dislocation by introducing tiny particles iron carbide

6.1.3 Mechanical Properties

- 1. Young's modulus: stress-strain ratio
- 2. The yield strength **s** is described by
- Hall-Petch equation for a conventional grain-size materials
- $\mathbf{s = s_0 + K / d^{0.5}}$
- Materials having smaller grains have more grain boundaries, blocking dislocation movement
- 3. Bulk nanostructured materials are quite brittle and display reduced ductility (~ a few % elongations) for grain size < 30 nm. Due to flaws and porosity

6.1.4 Nanostructured multilayers

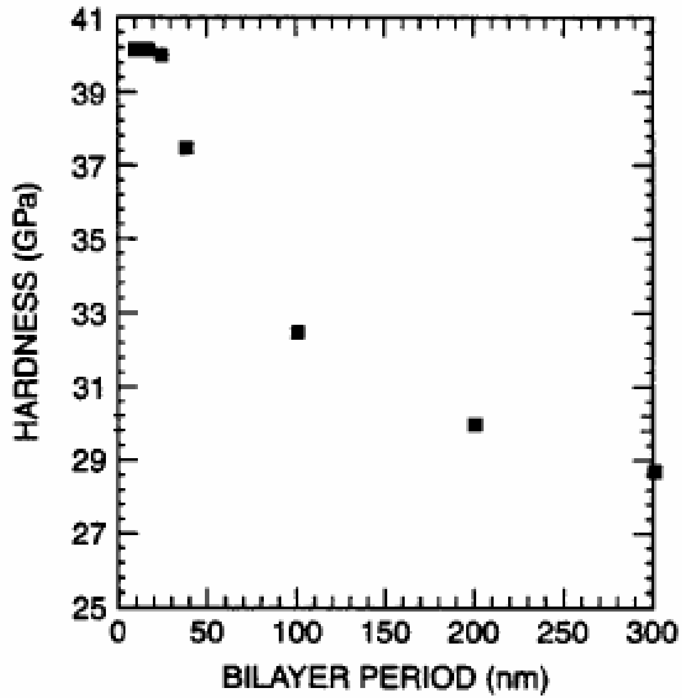

Figure 6.11. Plot of the hardness of TiN/NbN multilayer materials as a function of the thickness of the layers. (Adapted from B. M. Clemens, MRS Bulletin, Feb. 1999, p. 20.)

Due to Increasing interfaces and structure mismatch

6.1.5 Electrical properties

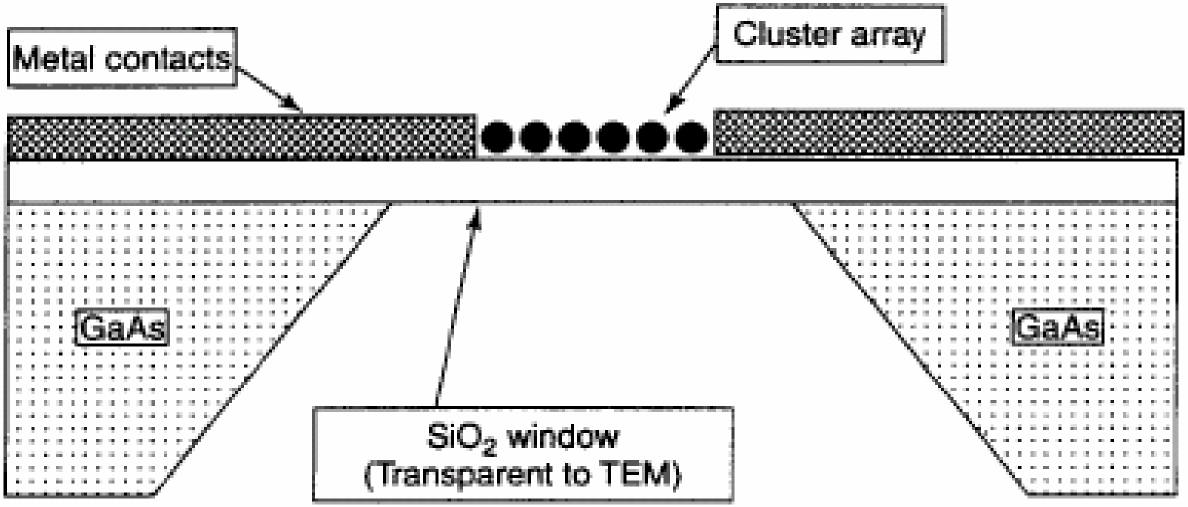

Figure 6.12. Cross-sectional view of a lithographically fabricated device to measure the electrical conductivity in a two-dimensional array of gold nanoparticles linked by molecules. (With permission from R. P Andres et al., in *Handbook of Nanostructured Materials and Nanotechnology*, H. S. Nalwa, ed., Academic Press, San Diego, 2000, Vol. 3, Chapter 4, p. 217.

$$G = G_o \exp\left(\frac{-E}{k_B T}\right)$$

E: activation energy

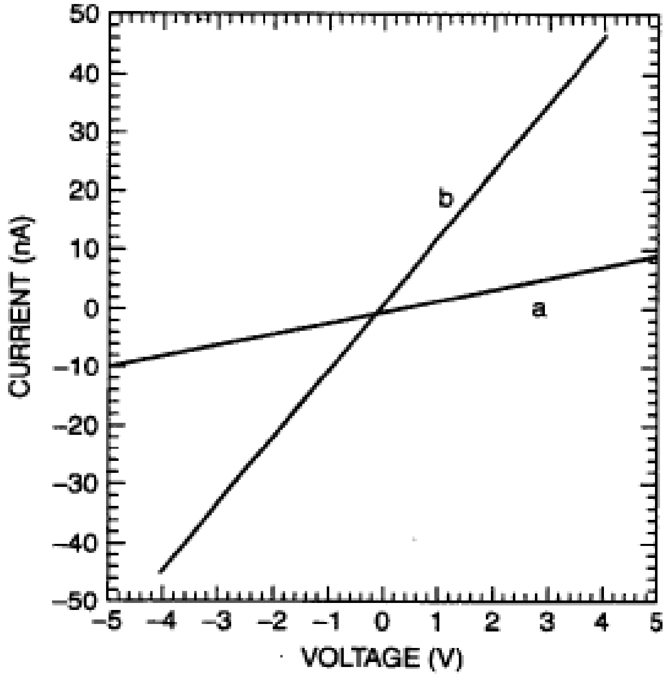

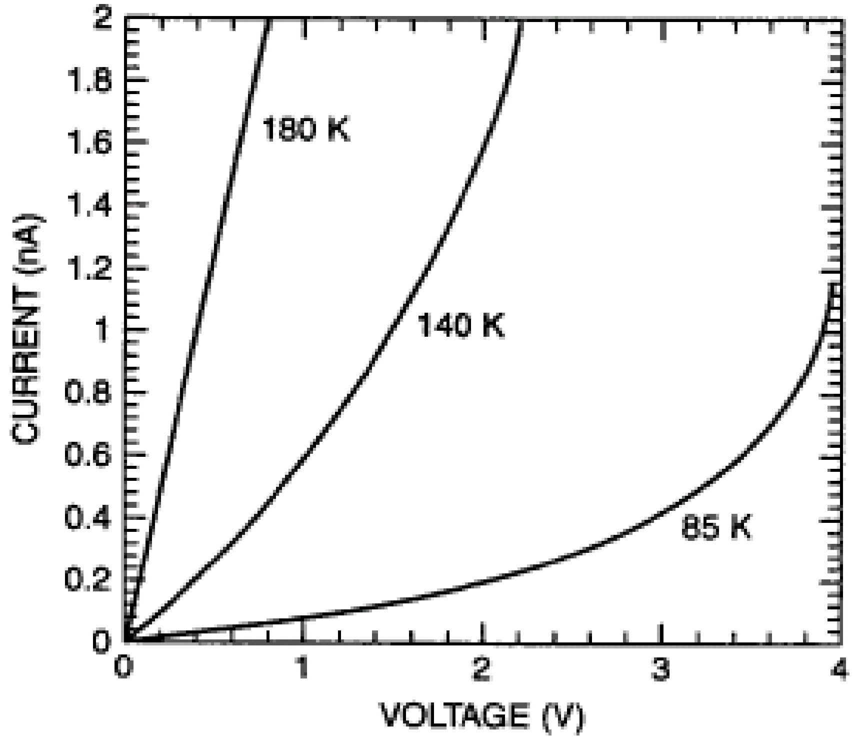

oom-temperature current–voltage relationship for a two-dimen
kage (line a) and with the particles linked by a $(CN)_2C_{18}H_{12}$ molecule (line b).

Electron tunneling

6.1. SOLID DISORDERED NANOSTRUCTURES 145

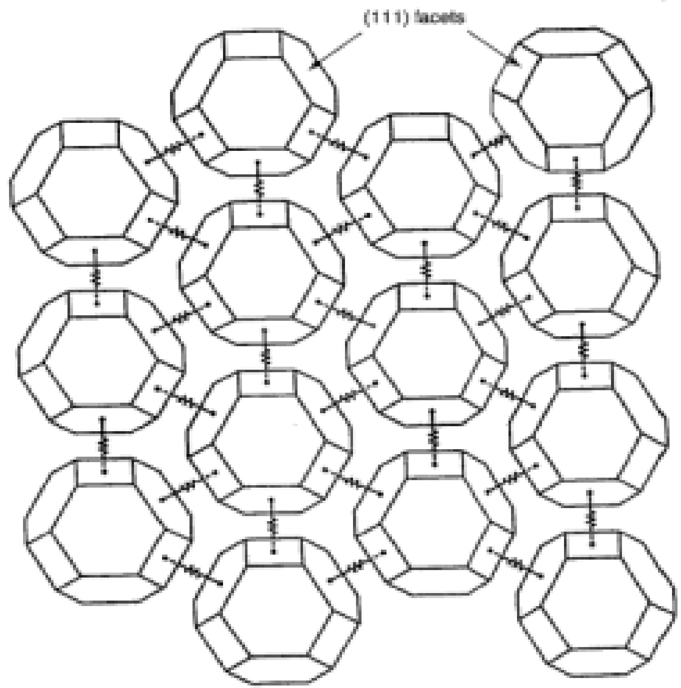

Figure 6.15. Sketch of a model to explain the electrical conductivity in an ideal hexagonal array of single-crystal gold clusters with uniform intercluster resistive linkage provided by resistors

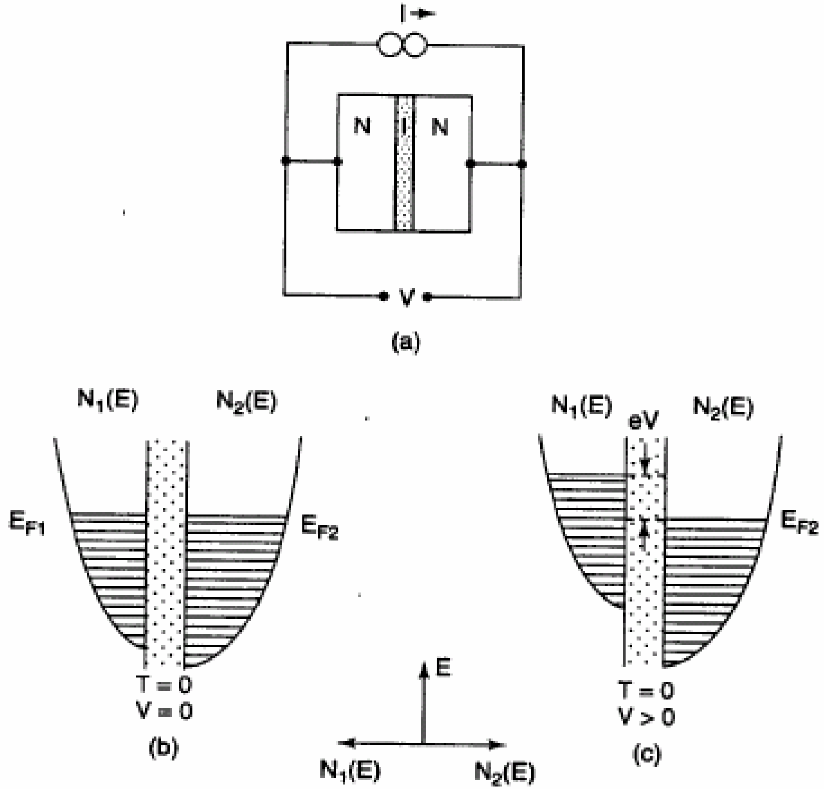

.16. (a) Metal–insulator–metal junction; (b) density of states of occupied leve

$$N_1(E - \mathrm{eV})f(E - \mathrm{eV})[N_2(E)(1 - f(E))] \qquad (6.3)$$

The no. of electrons that can move

$$I = K\int N_1(E - \mathrm{eV})N_2(E)[f(E - \mathrm{eV}) - f(E)]dE \qquad (6.4)$$

Net Current

$$G_{nn} = KN_1(E_f)N_2(E_f)e \qquad (6.7)$$

6.1.8 Porous Silicon made by electrochemical etching in hydrogen fluoride

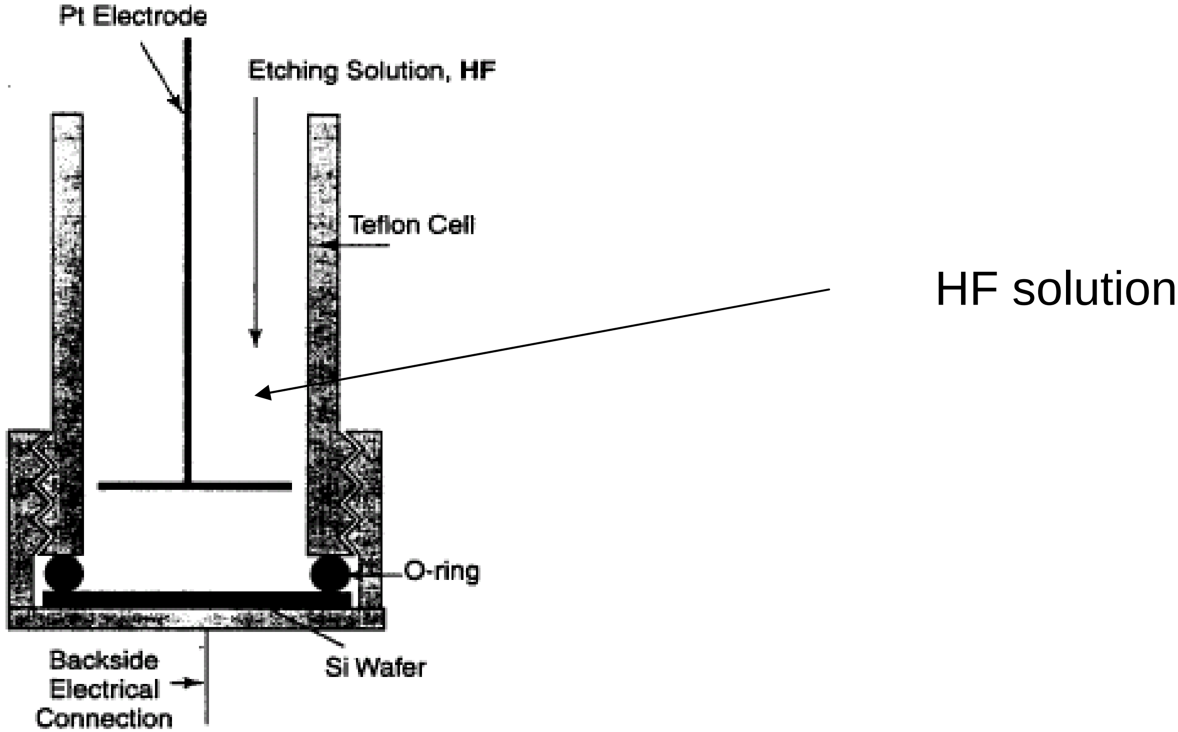

6.21. A cell for etching a silicon wafer in a hydrogen fluoride (HF) solution in order to ›e pores. (With permission from D. F. Thomas et al., in *Handbook of Nanostructured* *ls and Nanotechnology*, H. S. Nalwa, ed., Academic Press, San Diego, 2000, Vol. 4, r 3. p. 173.)

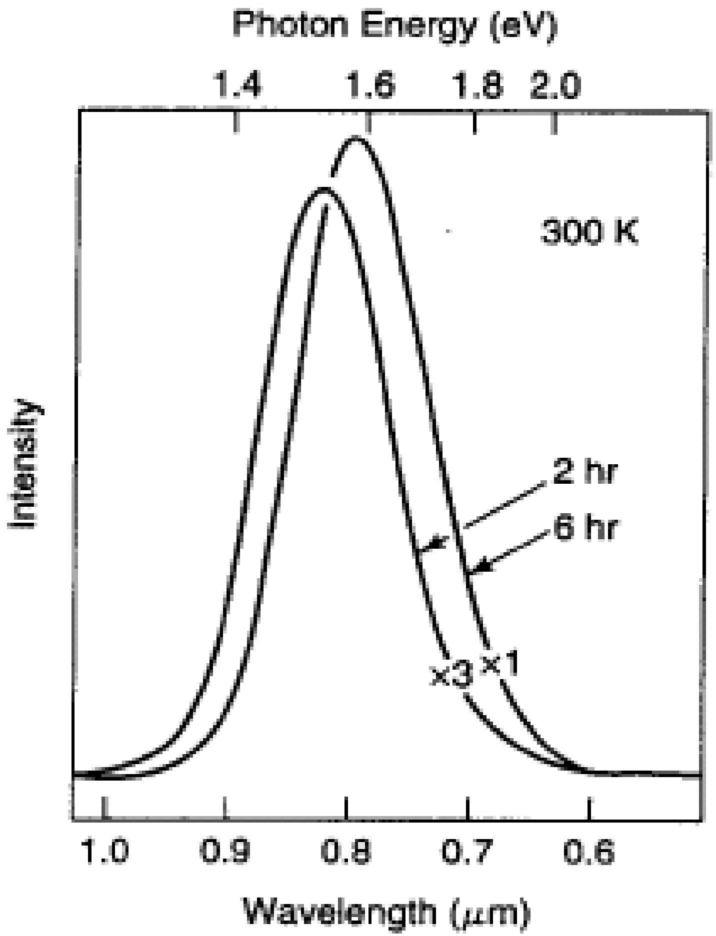

'uminescence spectra of porous silicon for two differe
lote the change in scale for the two curves. [Adapted f

Luminescence: Absorption of energy
Reemit Visible or near-visible light

Fluorescence: emission occurs within 10^{-8} s

Phosphorescence: a delay emission

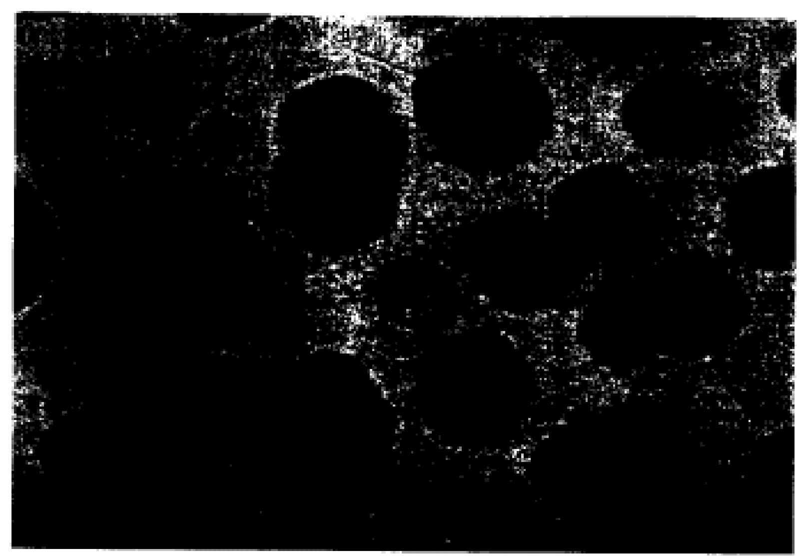

Explanations

p-type silicon is etched, a very fine network of pores having dimensions less than 10 nm is produced.

A number of explanations have been offered to explain the origin of the fluorescence of porous silicon, such as the presence of oxides on the surface of the pores that emit molecular fluorescence, surface defect states, quantum wires,

quantum dots and the resulting quantum confinement, and surface states on quantum dots. Porous silicon also displays electroluminscence, whereby the luminescence is induced by the application of a small voltage across electrodes mounted on the silicon, and cathodoluminescence from bombarding electrons.

Quantum effects 量子效應 ：

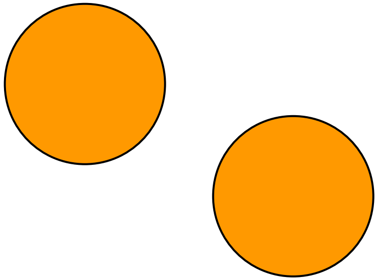

Quantum size effect
「量子尺寸效應」

Particles,etc

Quantum confinement effect
「量子侷限效應」

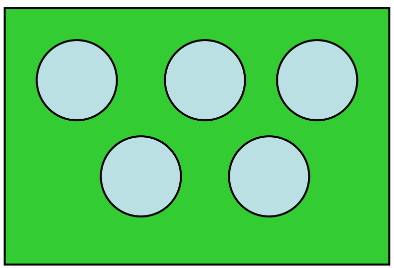

mesoporous materials,etc

Nanowire Growth Mechanism

- Vapor-Liquid-Solid
- Melt injection into porous templates
- ✓ Electrodeposition into porous templates

Fabrication of Porous Anodic Alumina Templates

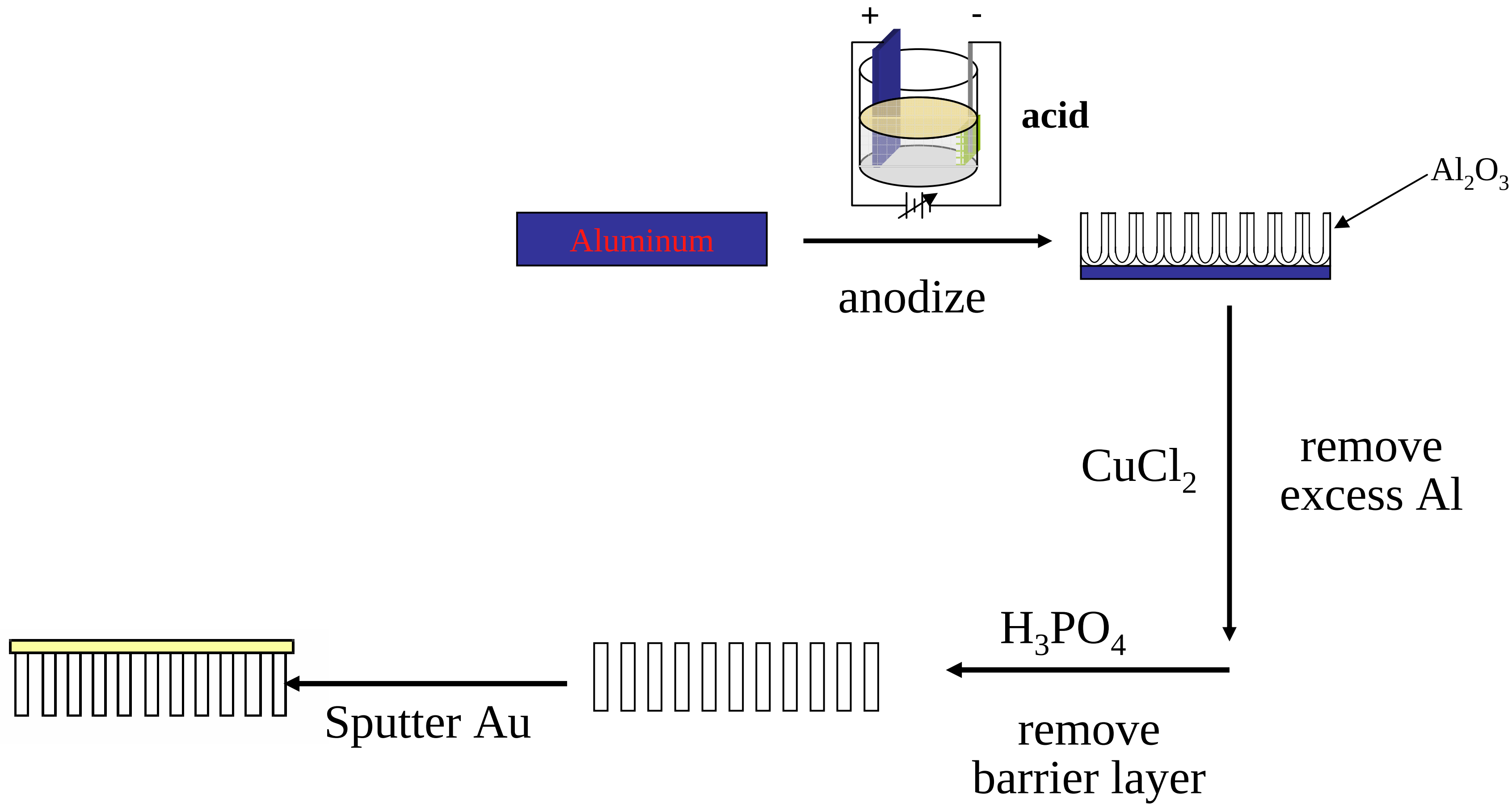

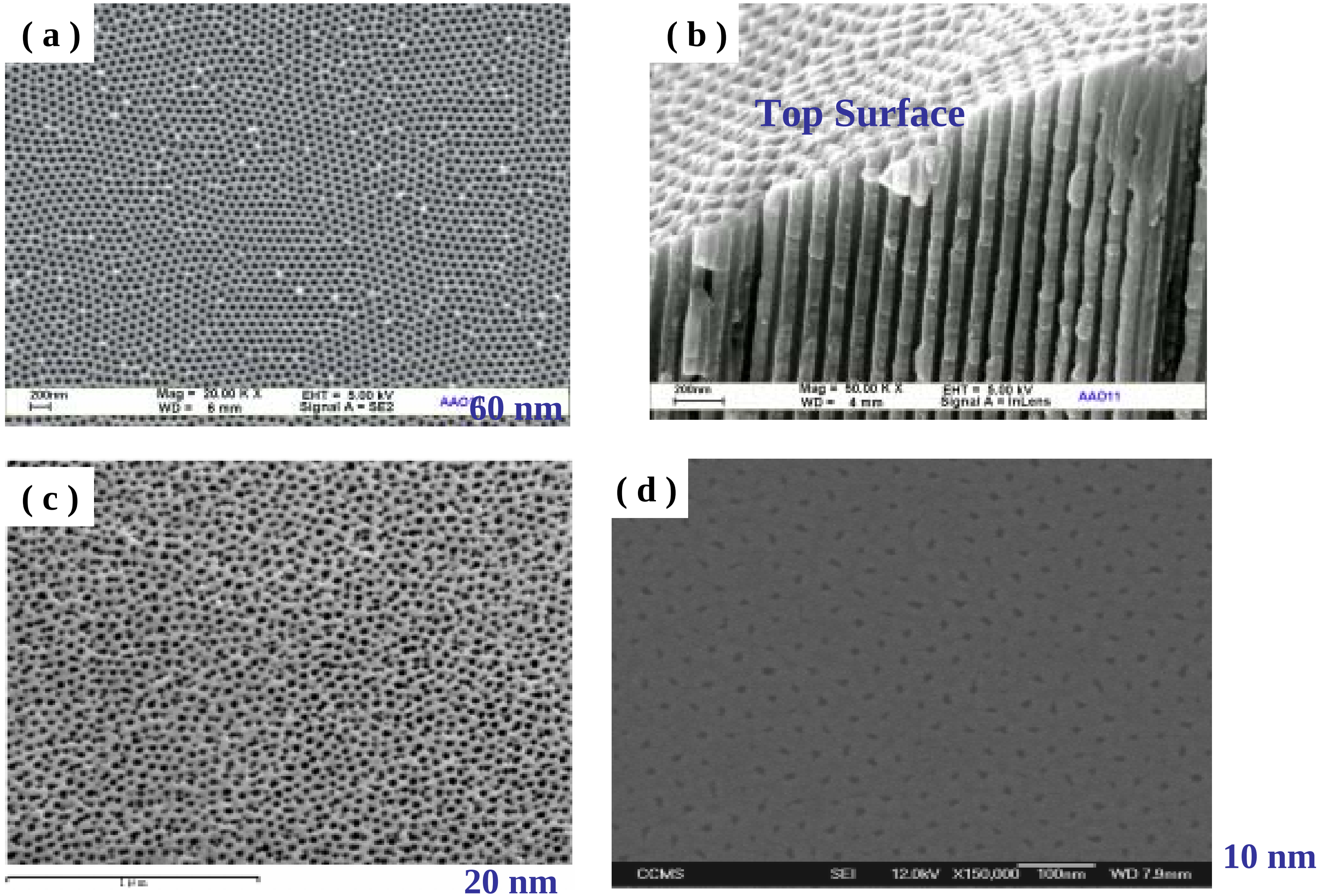

利用陽極處理氧化鋁 (Anodic Aluminum Oxide, AAO)製造各式尺寸的奈米孔洞模板, 孔洞的直徑分別為圖(a) 60nm (b)60nm nanopore template 的側面圖. (c)20nm (d) 10nm.

Electrodeposition of Bi2Te3 nanowire arrays

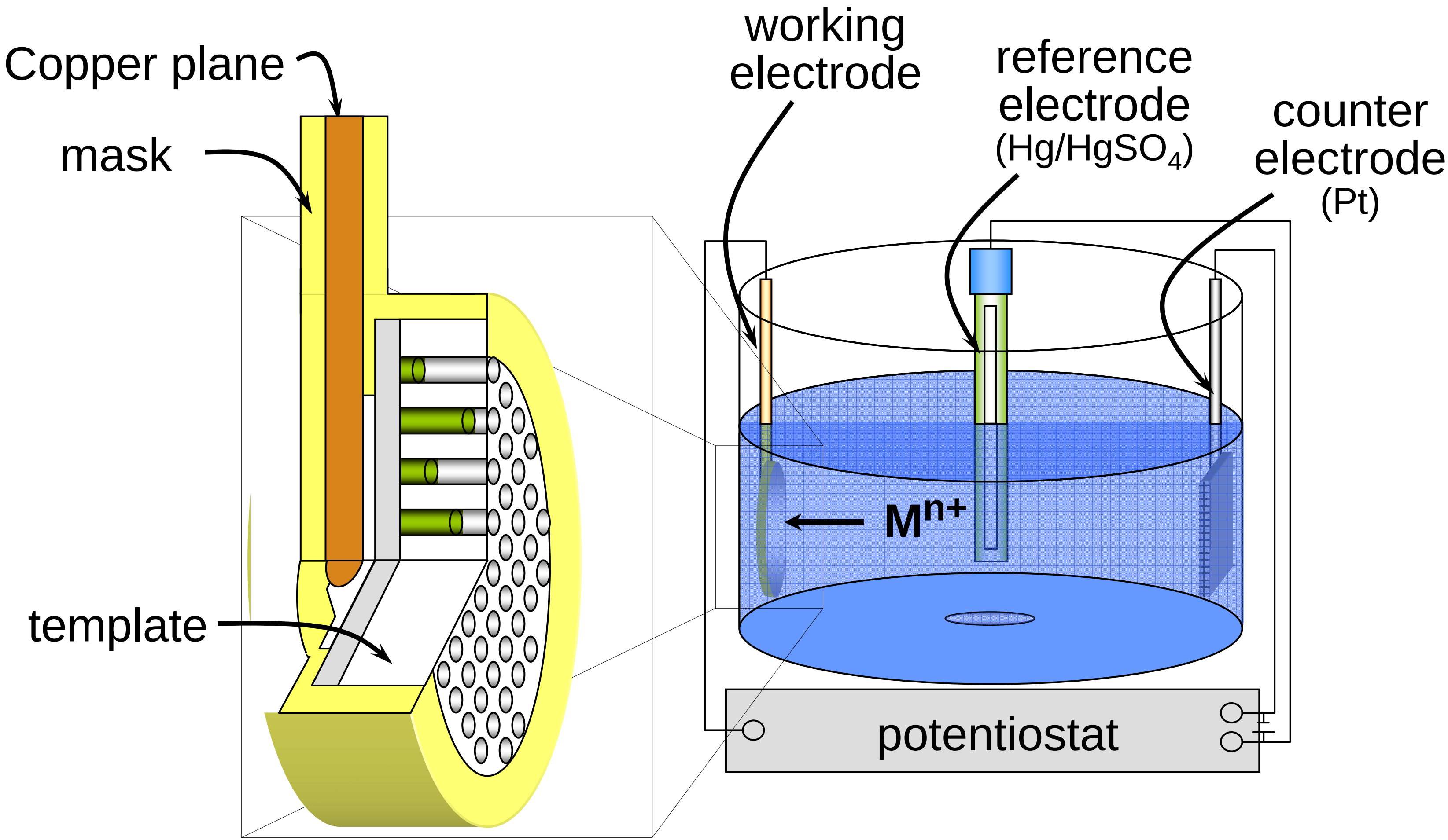

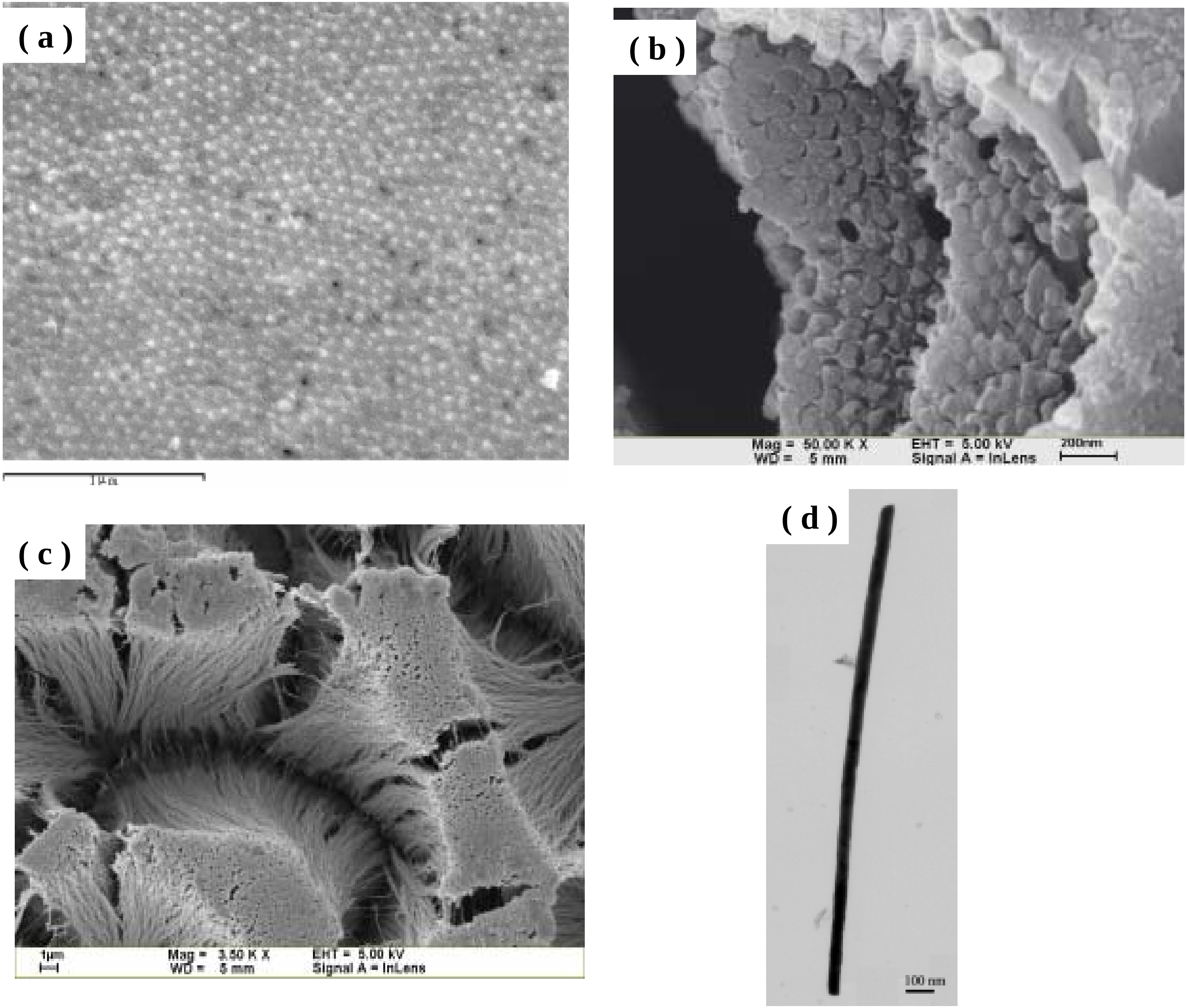
(a)
(b)
Mag = 50.00 K X
WD = 5 mm
EHT = 5.00 kV
Signal A = InLens
200nm
(c)
1μm
Mag = 3.50 K X
WD = 5 mm
EHT = 5.00 kV
Signal A = InLens
(d)
100 nm

Synthesis of Bi_2Te_3/alumina nanocomposites

UC, Berkley

Empty template - 75 nm pore diameter

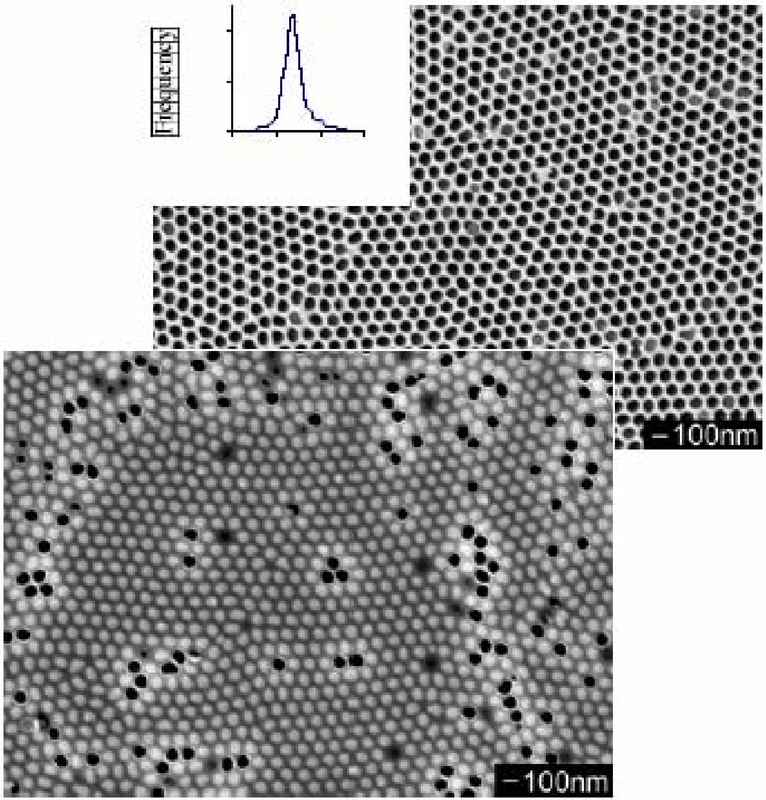

Filled template - 75 nm pore diameter

Empty template - 25 nm pore diameter

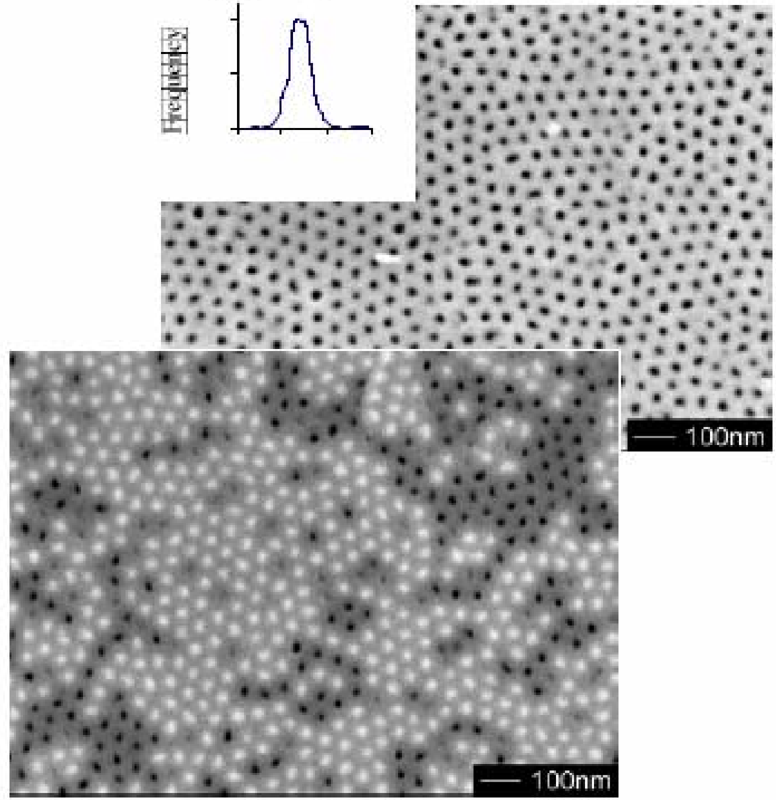

Filled template - 25 nm pore diameter

M.S. Sander, R. Gronsky, T. Sands, A.M. Stacy, "Structure of Bismuth Telluride Nanowire Arrays fabricated by Electrodeposition into Porous Anodic Alumina Templates," *Chem. Mater.* **15** (2003) pp. 335-39

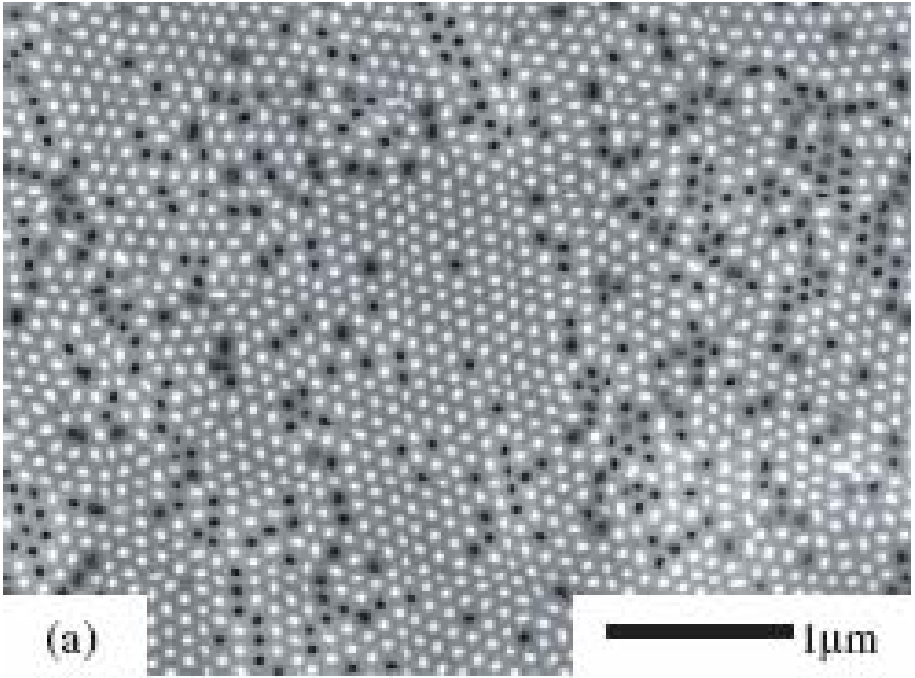

Bi2Te3 nanowire arrays (~45 nm)

(A. M. Stacy. Group, U. C. Berkeley. 2002)

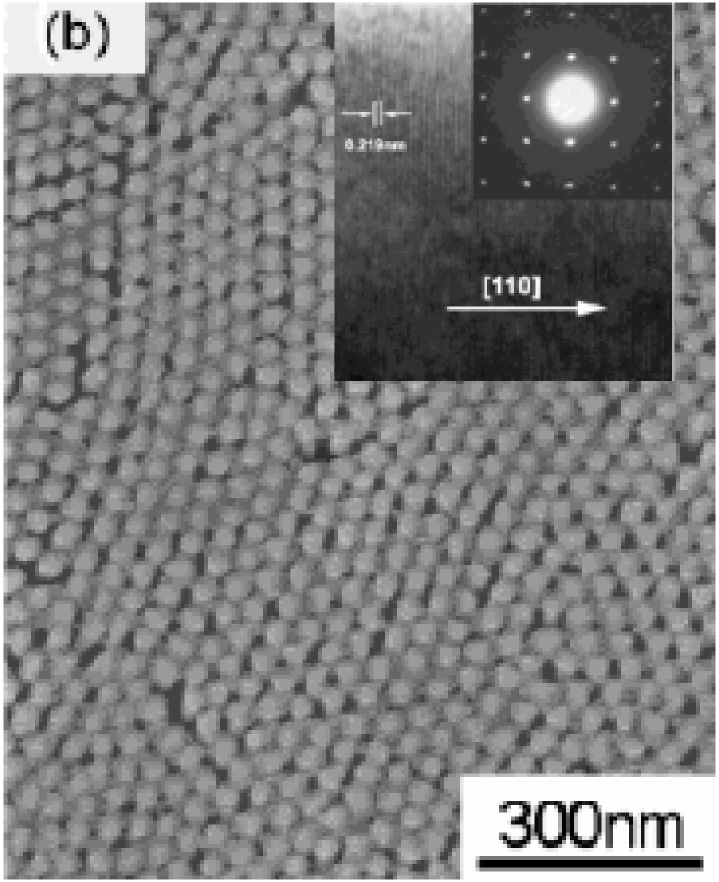

Hexagonal Bi2Te3 single-crystal Nanowires.

(**Xiaoguang Li, *Hefei*, P. R. China**)

J. Phys. Chem. B **2004,** *108,* 1844-1847

6.2 Nanostuctured Crystals

- Natural Nanocrystal
- B12

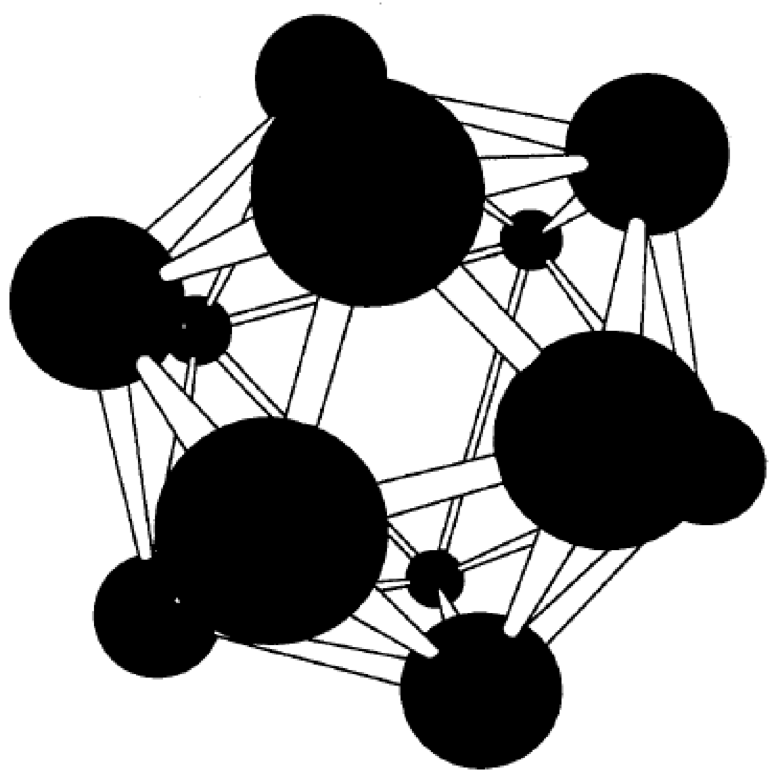

ıre 6.22. The icosohedral structure of a boron cluster containing 12 atoms. This
ɔasic unit of a number of boron lattices.

Fullerence C60

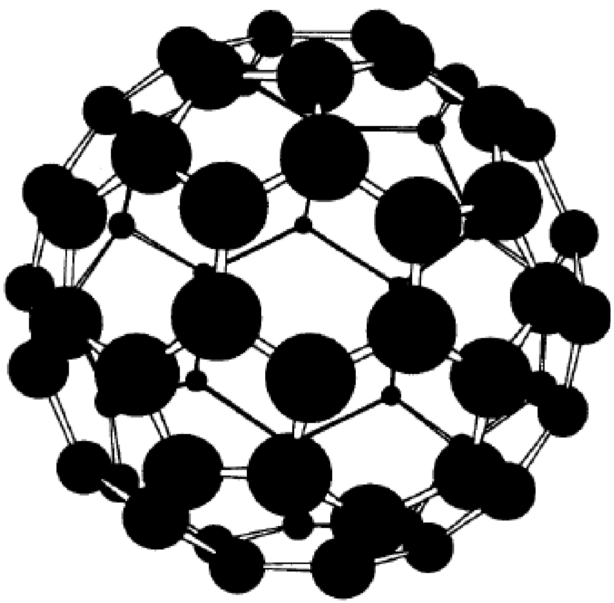

Figure 5.6. Structure of the C_{60} fullerene molecule.

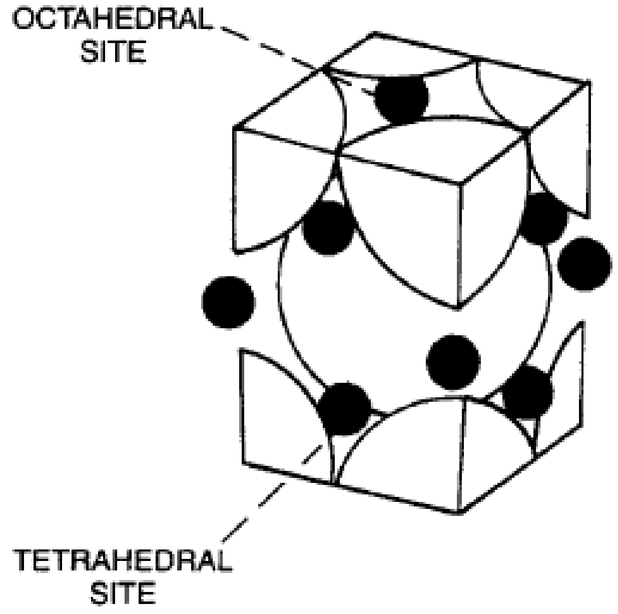

rystal lattice unit cell of C_{60} molecules (large spheres) doped with alkali atoms